

# Magnetic field of the roAp star KIC 10685175: observations versus theory

Fangfei Shi<sup>1,2</sup>, Huawei Zhang<sup>1,2</sup>, Svetlana Hubrig<sup>3</sup>, Silva Järvinen<sup>3</sup>, Huiling Chen<sup>1,2</sup>, Tianqi Cang<sup>4</sup>, Jianning Fu<sup>4,5</sup>, and Donald Kurtz<sup>6,7</sup>

<sup>1</sup> Department of Astronomy, Peking University, Beijing 100871, China  
e-mail: fangfei.1420@pku.edu.cn, zhanghw@pku.edu.cn

<sup>2</sup> The Kavli Institute for Astronomy and Astrophysics, Peking University, Beijing 100871, China

<sup>3</sup> Leibniz-Institut für Astrophysik Potsdam (AIP), An der Sternwarte 16, 14482 Potsdam, Germany

<sup>4</sup> School of Physics and Astronomy, Beijing Normal University, Beijing 100875, China

<sup>5</sup> Institute for Frontiers in Astronomy and Astrophysics, Beijing Normal University, Beijing 102206, China

<sup>6</sup> Centre for Space Research, North-West University, Mahikeng 2745, South Africa

<sup>7</sup> Jeremiah Horrocks Institute, University of Central Lancashire, Preston PR1 2HE, UK

October 1, 2024

## ABSTRACT

**Context.** KIC 10685175 is a roAp star whose polar magnetic field is predicted to be 6 kG through a non-adiabatic axisymmetric pulsation theoretical model.

**Aims.** In this work, we aim to measure the magnetic field strength of KIC 10685175 using high-resolution spectropolarimetric observations, and compare it with the one predicted by the theoretical model.

**Methods.** Two high-resolution unpolarized spectra have been analyzed to study for the presence of the magnetically split lines and derive the [Fe/H] ratio of this star through equivalent width measurements of ten Fe lines. One polarized spectrum has been used to measure the mean longitudinal magnetic field with the Least-Squares Deconvolution technique. Further, to examine the presence of chemical spots on the stellar surface, we have measured the mean longitudinal magnetic fields using different lines belonging to different elements.

**Results.** From the study of two high-resolution unpolarized spectra, we obtained  $[T_{\text{eff}}, \log g, [\text{Fe}/\text{H}], [\alpha/\text{Fe}], V_{\text{mic}}] = [8250 \pm 200 \text{ K}, 4.4 \pm 0.1, -0.4 \pm 0.2, 0.16 \pm 0.1, 1.73 \pm 0.2 \text{ km s}^{-1}]$ . Although the Fe absorption lines appear relatively weak in comparison to typical Ap stars with similar  $T_{\text{eff}}$ , the lines belonging to rare earth elements (Eu and Nd) are stronger than that in chemically normal stars, indicating the peculiar nature of KIC 10685175. The mean longitudinal magnetic field  $\langle B_{\ell} \rangle = -226 \pm 39 \text{ G}$  has been measured in the polarized spectrum, but magnetically split lines were not detected. No significant line profile variability was evident in our spectra. Also the longitudinal magnetic field strengths measured using line masks constructed for different elements have been rather similar. Due to a poor rotation phase coverage of our data, additional spectroscopic and polarimetric observations are needed to allow us to conclude on the inhomogeneous element distribution over the stellar surface.

**Conclusions.** The estimated polar magnetic field is  $4.8 \pm 0.8 \text{ kG}$ , which is consistent with the predicted polar magnetic field strength of about 6 kG within  $3\sigma$ . This work therefore provides support for the pulsation theoretical model.

**Key words.** stars: chemically peculiar - stars: magnetic field - stars: chemical abundance - Stars: individual: KIC 10685175

## 1. Introduction

Ap stars are chemically peculiar (CP) stars of spectral types A which have overabundances of iron-peak and rare-earth elements, such as Si, Cr, Sr, and Eu (Preston 1974). A prime factor governing the peculiarities of Ap stars is the strong magnetic fields they host. These magnetic fields are roughly dipolar with typical field strengths of a kG, or more. The strong magnetic field suppresses convection, thus providing a stable environment for ions with many absorption features to be lifted by radiation pressure against gravity and kept stratified in the observable surface layers. At the same time, some other elements, especially helium, that have few absorption lines near flux maximum in the

outer envelope of the star settle down affected by gravity. The element stratification in the presence of a magnetic field causes the peculiarities of surface abundance.

Some Ap stars exhibit high-overtone, low-degree pressure pulsation modes. These are called rapidly oscillating Ap (roAp) stars and they have many pulsation features. In the HR diagram, these stars overlap with  $\delta$  Sct stars which are non-magnetic (or extremely weakly magnetic). Generally, the  $\delta$  Sct stars pulsate in low overtone radial p modes while the roAp stars pulsate in high radial overtone magneto-acoustic modes. Also, unlike the non-magnetic stars, the pulsation axes of roAp stars are almost symmetric about the oblique quasi-dipolar magnetic field

(Kochukhov 2003; Saio 2005; Bigot & Kurtz 2011). Thus it is believed that the strong magnetic fields of roAp stars play an essential role in the pulsation mode excitation and selection (Balmforth et al. 2001; Saio 2005; Cunha 2006).

The pulsation axes of roAp stars are affected by the presence of a magnetic field as discussed in Dziembowski & Goode (1996), Cunha & Gough (2000), and Saio & Gautschy (2004), which means the pulsation mode is not a pure dipole or quadrupole (or higher). Saio (2005) provides a method to model the quadrupole or dipole pulsation distorted by dipole magnetic fields. In this model, the polar magnetic field is predicted by comparing the theoretical pulsation data with the observed one. Further, this model is used to estimate the polar magnetic field strength, effective temperature, mass, and other stellar parameters (Holdsworth et al. 2016, 2018). On the other hand, a test of consistency between the field measurements and the predictions on the magnetic field strengths permits to support the theoretical model, or place new constraints on it.

KIC 10685175 is a roAp star that has been observed by both *Kepler* (Borucki et al. 2010; Koch et al. 2010) and the Transiting Exoplanet Survey Satellite (TESS; Ricker et al. 2015). Gray et al. (2016) first classified KIC 10685175 as an Ap star with spectral type A6 IV (Sr)Eu using a LAMOST (Zhao et al. 2012; Cui et al. 2012) low-resolution spectrum, and a second classification of A4V Eu was given by Hümmerich et al. (2018) using a high-resolution spectrum obtained at Stará Lesná Observatory. However, magnetic field measurements have not been carried out for this star yet. Shi et al. (2020) studied the rotation and pulsation features of this star. Using their values for the rotation period,  $P_{\text{rot}} = 3.1028$  d, and the estimated radius,  $R = 1.39 \pm 0.05 R_{\odot}$  from Gaia Collaboration et al. (2018), we obtain the equatorial rotation velocity  $v_{\text{eq}} = 22.7 \pm 0.8 \text{ km s}^{-1}$ . Assuming the inclination  $i = 60^{\circ}$  from the work of Shi et al. (2020) we get  $v \sin i = 19.6 \pm 0.7 \text{ km s}^{-1}$ . The uncertainty of  $\sin i$  is not considered since it cannot be derived through the pulsation theoretical model in Shi et al. (2020). From the theoretical model presented by Saio (2005), the predicted dipole magnetic field strength is about 6 kG, which is expected to be detectable in a high-resolution spectra. If this predicted magnetic field can be confirmed by observations, this star will belong to a group of roAp stars with rather strong surface magnetic fields.

There are two main observational strategies to measure the magnetic field: one is related to spectroscopic observations of the magnetically split lines and observations of circular polarization. High-resolution spectroscopic observations permit to determine the average surface magnetic field,  $\langle B \rangle$ , by measuring the splitting between the Zeeman components in magnetically sensitive lines. This method is simple and straightforward, but requires high resolution and signal-to-noise ratio (SNR). Another method to measure magnetic fields is high-resolution spectropolarimetric observations. This method allows us to measure the average over the stellar disc of the line-of-sight component of the magnetic vector, which is called the mean longitudinal magnetic field. The observations of circular polarization are the most widely used to measure magnetic fields in Ap star and it does not need very high SNR.

## 2. Observations and data reduction

The spectra were obtained using the Echelle Spectropolarimetric Device for the Observation of Stars (ESPaDOnS) on the 3.6-m Canada-France-Hawaii Telescope (CFHT). ESPaDOnS is a bench-mounted high-resolution echelle spectrograph and spectropolarimeter with wavelength coverage from 370 to 1050 nm

(Donati et al. 2006). There are two observation modes for ESPaDOnS – spectropolarimetric mode with a resolving power of  $R \sim 68\,000$  and spectroscopic mode with higher resolution up to  $R \sim 81\,000$ .

Two high-resolution ( $R \sim 81\,000$ ) spectra were obtained in spectroscopic mode on 2021 September 1. Using the exposure time of 1300 s for each spectrum we achieved the SNR of about 60 at 6120 Å. On 2022 October 20, a lower resolution ( $R \sim 68\,000$ ) circularly polarised spectrum in spectropolarimetric mode was obtained as a follow-up observation. The spectropolarimetric observation consisted of four sub-exposures observed at different positions of the quarter-wave retarder plate. Each sub-exposure time is 1600 s. The achieved SNR of integral light spectra at 6120 Å is 90. The data was reduced using LibreESpRIT (Donati et al. 1997), which is the pipeline built for the ESPaDOnS. The reduction includes optimal spectrum extraction and normalization. More detailed information on the observations is presented in Table 1.

For clarity, the phase folded light curve of KIC 10685175 is shown in Figure 1 and the rotation phases of three spectral observations are marked as dotted lines in the figure. The data, time zero-point,  $T_0 = \text{BJD } 2,458,711.21391$ , and the rotation period,  $P_{\text{rot}} = 3.1028$  d, are all from Shi et al. (2020).

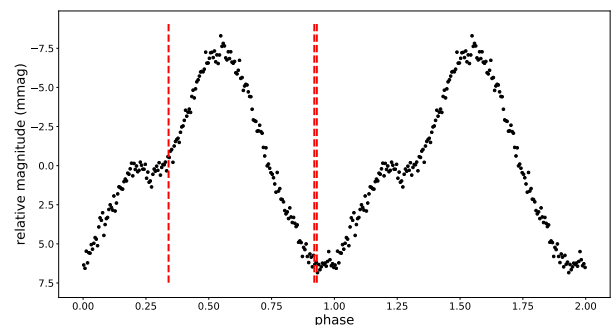


Fig. 1: The phase folded light curve of KIC 10685175. The positions of three spectral observations are marked as dotted lines in the figure.

## 3. Spectral analysis

The effective temperature,  $T_{\text{eff}}$ , and surface gravity,  $\log g$ , of KIC 10685175 have been measured in several works. Gaia Collaboration et al. (2018) derived  $T_{\text{eff}} = 7900$  K from *Gaia* DR2 Bp, Rp and G band photometry. Anders et al. (2022) derived  $T_{\text{eff}} = 8000$  K and  $\log g = 4.28$  using *Gaia* DR3 photometry together with other multi-bands of 2MASS and AllWISE. However, there are no stellar parameters based on high-resolution spectra for this star, and most measurements are from photometry and isochrone fitting. As LAMOST provides low-resolution spectra for this star, some works, such as Luo et al. (2022), derived  $T_{\text{eff}}$  and  $\log g$  based on low-resolution spectra. The parameters for this star found in the literature are listed in Table 2.

Here, we used the unpolarized spectra to derive the stellar parameters including  $T_{\text{eff}}$ ,  $\log g$ ,  $[\text{Fe}/\text{H}]$ ,  $[\alpha/\text{Fe}]$  and  $V_{\text{mic}}$  for KIC 10685175. In this paper, the value of  $\log g$  is in CGS system, and the unit of  $[\text{Fe}/\text{H}]$  and  $[\alpha/\text{Fe}]$  is dex.

The equivalent width (EW) measurements were performed using the program *iSpec* (Blanco-Cuaresma et al. 2014; Blanco-Cuaresma 2019). In the EW method, *iSpec* measures EWs of several selected lines by fitting them with Gaussian functions.

Table 1: Detailed information for the observations of KIC 10685175. The rotation phases are calculated based on the time zero-point  $T_0 = \text{BJD } 2,458,711.21391$  and the rotation period  $P_{\text{rot}} = 3.1028 \text{ d}$  from Shi et al. (2020).

HJD	Instrument	Resolution	SNR at 6120 Å	Mode	Exposure time (s)	Rotation phase
2459458.72644	ESPaDOnS	81 000	60	unpolarized	1300	0.92
2459458.78562	ESPaDOnS	81 000	60	unpolarized	1300	0.93
2459872.72369	ESPaDOnS	68 000	90	circularly polarized	1600×4	0.34

Table 2: The parameters of KIC 10685175 in the literature.

$T_{\text{eff}}$ (K)	$\log g$ (cgs)	[Fe/H] (dex)	Method	Reference
7900±100	-	-	three <i>Gaia</i> broad-band photometric measurements	Gaia Collaboration et al. (2018)
8000±280	4.28	-	Gaia EDR3 + 2MASS + AllWISE photometry	Anders et al. (2022)
8000	4.04	-0.11	KIC griz photometry	Pinsonneault et al. (2012)
8200±300	4.04	-0.11	KIC griz + 2MASS JHK + intermediate-bandD51 filter photometry	Huber et al. (2014)
8000±30	4.08	-0.03	LAMOST low-resolution spectrum	Luo et al. (2022)
7810±40	4.36	-0.07	LAMOST low-resolution spectrum	Xiang et al. (2022)
8000	4.20	-0.49		this work

Note:  $[\text{Fe}/\text{H}] = \log_{10}(N_{\text{Fe}}/N_{\text{H}}) - \log_{10}(N_{\text{Fe}}/N_{\text{H}})_{\odot}$ ,  $\log_{10} A(\text{Fe}) = \log_{10}(N_{\text{Fe}}/N_{\text{H}}) + 12$ , where  $A(\text{Fe})$  is the Fe abundance. In *iSpec*,  $A(\text{Fe})_{\odot}$  is 7.5, following Grevesse & Sauval (1998).

The theoretical EWs can be calculated considering the excitation equilibrium and ionization balance. A least-squares algorithm is applied in each iteration and the optimized parameters are selected by minimizing the differences between the observed and theoretical EWs.

The EW method requires unblended lines. We inspected Fe I and Fe II lines one by one to make sure that they are unblended and their EWs are smaller than 100 mÅ. Finally, 12 lines including 11 Fe I lines and one Fe II line were selected.

*iSpec* will derive Fe abundances based on the EW of each Fe line. The Fe abundances are assumed to be independent with reduced equivalent width ( $\log_{10} \frac{EW}{\lambda}$ ), the lower energy levels, the ionization states which is sensitive to micro-turbulence velocity, effective temperature,  $\log g$ , respectively.

Since we only have one Fe II line, it is unreliable to derive  $\log g$  based on the ionization balance. Here, we calculated  $\log g$  from photometry. Assuming  $T_{\text{eff}} = 8000 \text{ K}$ , with parallax and magnitude from *Gaia* DR3, we have  $\log g = 4.4 \pm 0.1$ .

We fixed  $\log g = 4.4$  and give initial values of  $T_{\text{eff}}$ , [Fe/H],  $[\alpha/\text{Fe}]$  and  $V_{\text{mic}}$ . We started from  $[T_{\text{eff}}, [\text{Fe}/\text{H}], [\alpha/\text{Fe}], V_{\text{mic}}] = [8000 \text{ K}, -0.1, 0.04, 2.5 \text{ km s}^{-1}]$ , where the initial values of  $T_{\text{eff}}$  and [Fe/H] are from the average values from Table 2,  $[\alpha/\text{Fe}] = -0.4[\text{Fe}/\text{H}]$  was calculated using the relationship in Matsuno et al. (2022), and  $V_{\text{mic}}$  was estimated using an empirical relation considering the effective temperature, surface gravity and metallicity which was constructed in *iSpec*. Then these four parameters were gradually changed to finally make sure that there is no trend between [Fe/H] and lower excitation energy; there is no trend between [Fe/H] and reduced EWs; and the final [Fe/H] is the average value of those of 12 lines.

Using the atomic line-list extracted from VALD, atmosphere model from ATLAS (Castelli & Kurucz 2004), and based on MOOG code (Snedden et al. 2012), we derived the final result  $[T_{\text{eff}}, [\text{Fe}/\text{H}], [\alpha/\text{Fe}], V_{\text{mic}}] = [8250 \pm 200 \text{ K}, -0.4 \pm 0.2, 0.16 \pm 0.1, 1.7 \pm 0.2 \text{ km s}^{-1}]$ . The uncertainties of  $T_{\text{eff}}$  and  $V_{\text{mic}}$  were decided from that the slopes  $-T_{\text{eff}}$  and  $V_{\text{mic}}$  the slopes of the trend of [Fe/H] v.s. lower excitation energy and [Fe/H] v.s. reduced equivalent width should be smaller than 0.1, the uncertainty of [Fe/H] was from standard deviation of those of 12 lines, and the uncertainty of  $[\alpha/\text{Fe}]$  was propagated from that of [Fe/H]. We also examined that the ionization equilibrium is satisfied using the fixed  $\log g = 4.4$ .

[Fe/H] = -0.4 is very different compared with the measurements in the literature, where the results have been derived from photometry and evolution models that are less suitable for Ap stars. The low [Fe/H] also indicates that the Fe abundance of this star is lower than that of an Ap star with  $T_{\text{eff}} = 8000 \text{ K}$ , although it is typical for Ap stars much cooler than KIC 10685175 (see fig. 5 of Ghazaryan et al. 2018.)

In the following we compared the spectrum of KIC 10685175 with another Ap star and an A type star with normal chemical abundance. The chemically normal star we chose is HD 186689, with fundamental parameters  $T_{\text{eff}} = 7950 \text{ K}$ ,  $\log g = 4.16$ , and [Fe/H] = -0.33 (Gaia Collaboration et al. 2016, 2023) which are similar to those of KIC 10685175. The  $v \sin i$  for this star is  $34 \text{ km s}^{-1}$  (Erspamer & North 2003), which is slightly larger than that of KIC 10685175. The spectrum was obtained from the ELODIE<sup>1</sup> database and is shown in Fig. 2. Compared with HD 186689, KIC 10685175 has slightly weaker Fe lines but Nd and Eu show significant overabundance, which is a typical feature for Ap stars. We also compared the spectrum of KIC 10685175 with the spectrum of another Ap star with similar  $T_{\text{eff}}$ ,  $\alpha$  Cir. The  $T_{\text{eff}} = 7900 \text{ K}$ ,  $\log g = 4.2$  and  $v \sin i = 13.2 \text{ km s}^{-1}$  of  $\alpha$  Cir (Ghazaryan et al. 2018; Ammler-von Eiff & Reiners 2012) are close to those of KIC 10685175. The spectrum of  $\alpha$  Cir was obtained by Holdsworth & Brunsten (2020) using the High Resolution Spectrograph (HRS) attached to the Southern African Large Telescope (SALT). In Figure 2, we show that for KIC 10685175, the Fe lines are much weaker than those in  $\alpha$  Cir. For Eu and Nd lines, by calculating equivalent widths of each line, we confirmed that two stars have similar intensities for Eu II line, and the Nd III line of KIC 10685175 is less enhanced.

## 4. The magnetic field of KIC 10685175

### 4.1. The surface magnetic field

High-resolution spectroscopic observations can be used to determine the mean magnetic field modulus,  $\langle B \rangle$  (Mathys 1989), by measuring the wavelength shifts between the magnetically split components using the relation:

<sup>1</sup> <http://atlas.obs-hp.fr/elodie/>

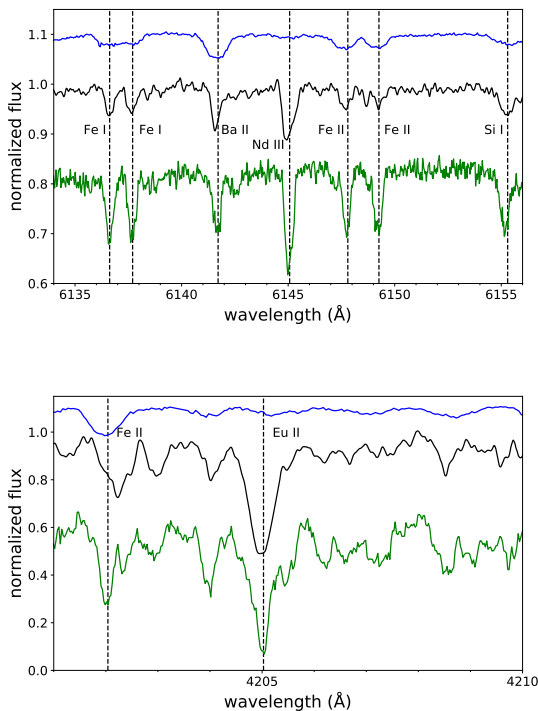


Fig. 2: Comparison of the spectra in the vicinity of the Nd and Eu lines between three A-type stars: the spectrum the star with normal abundance, HD 186689 (top – blue), our target, KIC 10685175 (middle – black), and the spectrum of the known  $\alpha$  Cir star,  $\alpha$  Cir (bottom – green). Strong spectral lines are marked with black dashed lines. The abscissa is wavelength in ( $\text{\AA}$ ) and the ordinate is normalized intensity. For clarity, the spectra of HD 186689 and  $\alpha$  Cir are shifted.

$$\lambda_r - \lambda_b = gk\lambda_0^2 \langle B_\ell \rangle. \quad (1)$$

Here,  $\lambda_r$ ,  $\lambda_b$ , and  $\lambda_0$  represent the wavelength of the red, and blue components, and the central wavelength, respectively;  $g$  is the Landé factor, and  $k = 4.67 \times 10^{-13} \text{ \AA}^{-1} \text{ G}^{-1}$ .

The widely used magnetically sensitive doublet Fe II 6149  $\text{\AA}$  has been inspected for the presence of magnetically split lines. However, as we show in Fig. 3, this line does not exhibit magnetically split structure. We also have inspected other magnetically sensitive lines which have large Landé factors ( $g_{\text{eff}} \geq 1.5$ ) and doublet patterns, such as Fe I 6336.82  $\text{\AA}$  ( $g_{\text{eff}} = 2.0$ ) and Cr II 5116.04  $\text{\AA}$  ( $g_{\text{eff}} = 2.92$ ), but no magnetically split pattern are detected. The relatively high  $v \sin i$  for this star significantly inhibits the detection of magnetically split lines. Besides, the profile variation due to the spots can also contaminate the line splitting or broadening from the Zeeman effect, which makes the line splitting less likely to be detected.

#### 4.2. The longitudinal magnetic field

The reduced circularly polarized observations provide Stokes intensity  $I$ , circular polarization  $V$  parameters, and diagnostic  $N$  spectra. The mean longitudinal magnetic field,  $\langle B_\ell \rangle$ , is determined through:

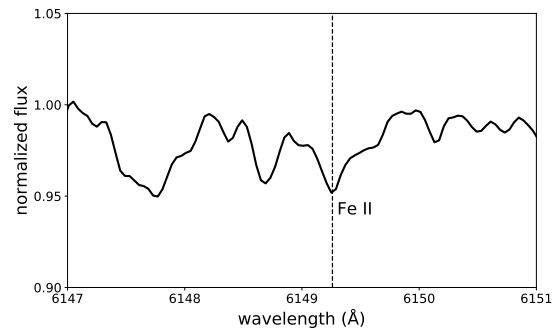


Fig. 3: The combined spectrum ( $R = 81\,000$ ) of KIC 10685175 zoomed in the spectral region containing the magnetically sensitive line Fe II 6149  $\text{\AA}$ .

$$\langle B_\ell \rangle = -2.14 \times 10^{11} \frac{\int vV(v)dv}{\lambda_0 g_{\text{eff}} c \int [I_c - I(v)]dv}. \quad (2)$$

Here,  $v$  is the velocity offset from the line center, and the unit is  $\text{km s}^{-1}$ ;  $\lambda_0$  and  $g_{\text{eff}}$  are the effective wavelength and the effective Landé factor used for normalization, respectively (Rees & Semel 1979; Donati et al. 1997).

The noise level is greatly reduced with the help of the Least Square Deconvolution technique (LSD; Donati et al. 1997; Folsom et al. 2018). In this technique it is assumed that each spectral line can be described by the same profile with a different scale factor which depends on the central wavelength, the line strength, and the magnetic sensitivity.

The line list was constructed using the Vienna Atomic Line Database (VALD; Ryabchikova et al. 2015) assuming  $T_{\text{eff}} = 8200 \text{ K}$  and  $\log g = 4.4$ . All the lines were inspected to make sure that they are deeper than 5% of the continuum and not significantly blended with other lines. Lines contaminated by telluric absorption or located in hydrogen line wings were removed from the line list. The information about the selected line list is presented in Table 3.

In Fig. 4, we show for the line list constructed for all elements the LSD profiles of Stokes  $I$ ,  $V$ , and diagnostic null. LSD profiles were calculated in the velocity range of  $-30$  to  $30 \text{ km s}^{-1}$  using a step of  $1 \text{ km s}^{-1}$ . The normalized Landé factor is 1.26, and the normalized wavelength of 4914  $\text{\AA}$ . We followed the generally adopted procedure to use the false alarm probability (FAP) based on reduced  $\chi^2$  test statistics (Donati et al. 1992, 1997): the presence of a Zeeman signature is considered as a definite detection (DD) if  $\text{FAP} \leq 10^{-5}$ , as a marginal detection (MD) if  $10^{-5} < \text{FAP} \leq 10^{-3}$ , and as a non-detection (ND) if  $\text{FAP} > 10^{-3}$ . The  $V$  spectrum exhibits a clear Zeeman feature indicating the presence of a magnetic field. Using Eq. 2, the mean longitudinal magnetic field is calculated to be  $\langle B_\ell \rangle = -226 \pm 39 \text{ G}$ . The FAP is listed in Table 3.

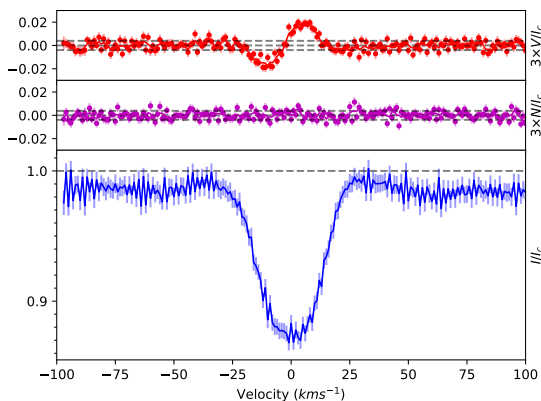
#### 4.3. The comparison of the measured and the predicted magnetic field strengths

In the recent study of Shi et al. (2020) it was suggested that KIC 10685175 possess a strong magnetic field with the dipole magnetic field strength of 6 kG. The theoretical pulsation model of Saio (2005) was used to compare the observations of KIC 10685175 with theoretical predictions. Following Stibbs



Table 3: Numbers of the lines in line lists and the mean longitudinal magnetic field calculated from different elements.

Element	Number of lines	The mean depth	The mean Landé factor	The mean wavelength (Å)	The mean longitudinal magnetic field (G)	FAP	Detectable
all	208	0.49	1.26	4914	$-226 \pm 39$	$1.7 \times 10^{-6}$	DD
Ca I	28	0.51	1.18	5358	$-115 \pm 57$	0.011	ND
Cr II	20	0.46	1.20	4718	$-398 \pm 105$	$8 \times 10^{-4}$	MD
Fe I	75	0.49	1.33	5009	$-248 \pm 47$	$6 \times 10^{-6}$	DD
Fe II	21	0.61	1.14	4798	$-254 \pm 55$	$6 \times 10^{-4}$	MD

Fig. 4: The profile of Stokes  $V$ , diagnostic null, and  $I$  (from top to bottom) calculated for KIC 10685175.

(1950), and assuming a dipole magnetic field inclined by an angle  $\beta$  to the rotation axis, a polar magnetic field can be estimated through:

$$B_{\ell} = \frac{1}{20} \frac{15 + u}{3 - u} B_p (\cos \beta \cos i + \sin \beta \sin i \cos(2\pi\Phi)). \quad (3)$$

The limb darkening coefficient  $u = 0.5$  was extracted from Claret & Bloemen (2011), using  $\log g = 4.5$ ,  $T_{\text{eff}} = 8000$  K and metallicity  $Z = 0$ . The value  $Z$  was derived through  $Z = 10^{[\text{Fe}/\text{H}]} \times Z_{\odot}$ , where  $[\text{Fe}/\text{H}] = -0.4$  and  $Z_{\odot} = 0.02$ . Using the mean longitudinal magnetic field strength  $B_{\ell} = -226 \pm 39$  G determined in the rotational phase  $\Phi = 0.34$ , the stellar inclination and the magnetic obliquity,  $(i, \beta) = (60^{\circ}, 60^{\circ})$ , from the pulsation model presented in Shi et al. (2020), we estimated the polar magnetic field to be  $4.8 \pm 0.8$  kG. This is compatible with the theoretically predicted polar magnetic field of 6 kG within  $3\sigma$  supporting the theoretical model of Saio (2005).

## 5. Discussion and conclusion

Using two high-resolution spectroscopic spectra and one circularly polarized spectrum we have studied the stellar parameters of the roAp star KIC 10685175 and measured its mean longitudinal magnetic field strength. Compared to chemically normal stars, KIC 10685175 exhibits chemical peculiarities such as overabundance of Eu and Nd which is typical of magnetic Ap stars. Fe lines however appear weaker than in other Ap stars with similar fundamental parameters.

Due to the lower number of available spectra, it is difficult to conclude whether chemical spots are present on the stellar surface. An inhomogeneous surface element distribution can be explored by considering the differences in magnetic field strengths

obtained using line lists constructed for different elements. Assuming a dipolar magnetic field configuration, if a stronger mean longitudinal magnetic field is measured in the lines of a specific element, we can conclude that this element tends to form a spot closer to the magnetic pole. The results of the LSD technique applied to the line masks for Ca I, Cr II, Fe I and Fe II are displayed in Fig. 5 and the results of our measurements of the mean longitudinal magnetic field are presented in Table 3. Unfortunately, due to the low number of unblended lines belonging to the rare earth elements, no corresponding line lists have been constructed. Hümmerich et al. (2018) classified KIC 10685175 as A4V Eu. However, there are too few Eu lines visible in the spectrum to construct an Eu line mask.

As we show in Table 3, only the mean longitudinal magnetic field using Fe I lines is definitely detected and the result,  $B_{\ell}(\text{Fe I}) = -248 \pm 47$  G, is very close to the measurements obtained using all lines. This is reasonable because the number of Fe I lines dominates the line list. For Ca I, we obtained  $B_{\ell}(\text{Ca I}) = -115 \pm 57$  G, but the FAP indicates no detection. The magnetic fields for Fe II ( $-254 \pm 55$  G) and Cr II ( $-398 \pm 105$  G) are only marginally detected. The difference between the magnetic field strengths obtained for Cr II, Fe I and Fe II is larger than  $1\sigma$ . It may probably be due to the inhomogeneous distribution of these elements, but is not significant enough to make a solid conclusion.

Chemical spots on the surface of Ap stars usually cause significant variability of the spectral line profiles over the rotation period (Babcock 1958). To further test the possible presence of chemical spots on the surface of KIC 10685175, the LSD technique has been applied for all three available observations to calculate the Stokes  $I$  profiles. Using the time zero point  $T_0 = \text{BJD } 2,458,711.21391$  and the rotation period  $P_{\text{rot}} = 3.1028$  d from Shi et al. (2020), both unpolarized spectra correspond to the rotation phases 0.92 and 0.93, respectively, and the polarized spectrum to the phase 0.34. For all three different rotation phases the Stokes  $I$  profiles calculated for the line list containing all lines and those for the line lists constructed for different elements are presented in Fig. 6 and Fig. 7. We also checked the Stokes  $I$  profiles for Nd and Pr, but only Nd III 6145 Å can be detected in all spectra. So in Fig. 7, we compared the profiles of Nd III 6145 Å directly without calculating LSD profiles. No significant changes in the LSD Stokes  $I$  profiles are detected, although the profiles for Fe I calculated for the phase 0.34 show slightly flat-bottom profiles compared to those observed in other phases. As the rotation phase coverage of our data is rather poor, additional observations are needed to permit to conclude of the surface inhomogeneous element distribution.

Despite the fact that magnetically split lines were not detected in our spectra, under the assumption of the dipolar topology of the global magnetic field, the strength of the measured mean longitudinal magnetic field,  $\langle B_{\ell} \rangle = -226 \pm 39$  G in combination with already known stellar inclination and the magnetic

obliquity suggest the polar magnetic field to be  $4.8 \pm 0.8$  kG. This polar field strength is consistent with field strength predicted by the theoretical model of Saio (2005).

## Acknowledgements

This work was funded by the National Natural Science Foundation of China (NSFC Grant No.12090040, 12090042, 12090044, U1731108 and 11833002) and the National Key R&D Program of China (No. 2019YFA0405500). DWK acknowledges support

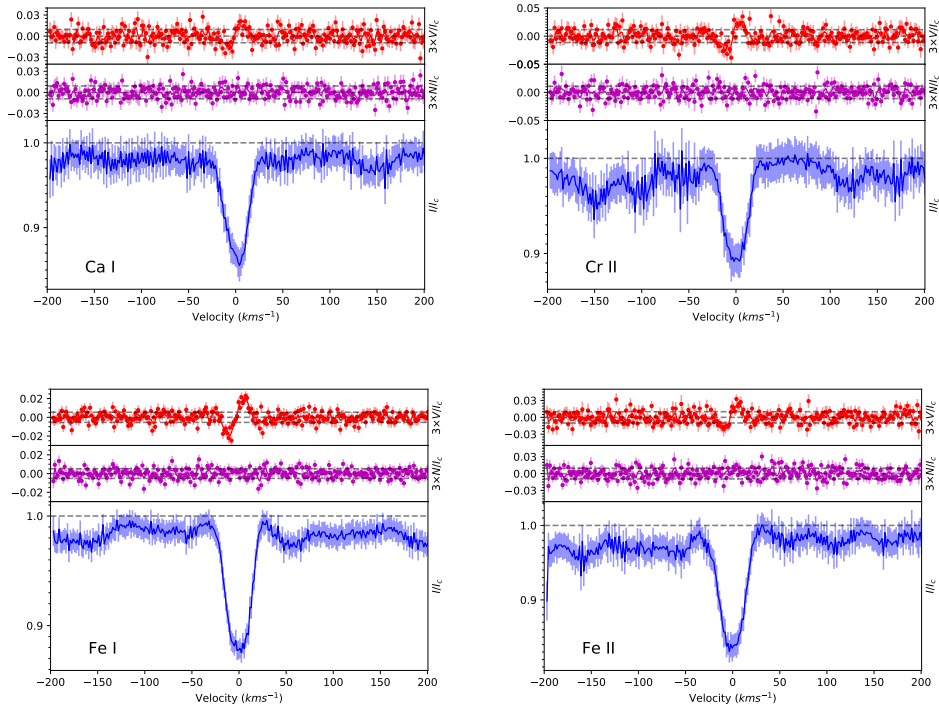


Fig. 5: Same as Fig. 4 but for different elements.

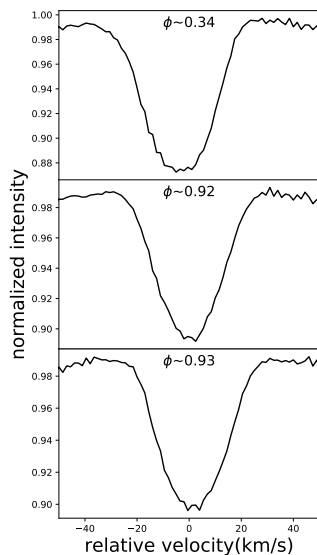


Fig. 6: The LSD Stokes  $I$  profiles calculated for all three available observations using all lines. Rotation phase are marked on the top of each panel.

from the Fundação para a Ciência e a Tecnologia (FCT) through national funds (2022.03993.PTDC).

This work is based on data collected at the Canada-France-Hawaii Telescope, and also uses data from the VALD database, European Space Agency mission *Gaia* (<http://www.cosmos.esa.int/Gaia>), and the SIMBAD database. The observation time is obtained through the Telescope Access Program (TAP).

Some of the observations in this paper were obtained with the Southern African Large Telescope (SALT) under proposal code 2017-1-SCI-023 (PI: Holdsworth).

## References

- Ammler-von Eiff, M. & Reiners, A. 2012, *A&A*, 542, A116  
 Anders, F., Khalatyan, A., Queiroz, A. B. A., et al. 2022, *A&A*, 658, A91  
 Babcock, H. W. 1958, *ApJS*, 3, 141  
 Balmforth, N. J., Cunha, M. S., Dolez, N., Gough, D. O., & Vauclair, S. 2001, *MNRAS*, 323, 362  
 Bigot, L. & Kurtz, D. W. 2011, *A&A*, 536, A73  
 Blanco-Cuaresma, S. 2019, *MNRAS*, 486, 2075  
 Blanco-Cuaresma, S., Soubiran, C., Heiter, U., & Jofré, P. 2014, *A&A*, 569, A111  
 Borucki, W. J., Koch, D., Basri, G., et al. 2010, *Science*, 327, 977  
 Castelli, F. & Kurucz, R. L. 2004, *New Grids of ATLAS9 Model Atmospheres*  
 Claret, A. & Bloemen, S. 2011, *A&A*, 529, A75  
 Cui, X.-Q., Zhao, Y.-H., Chu, Y.-Q., et al. 2012, *Research in Astronomy and Astrophysics*, 12, 1197  
 Cunha, M. S. 2006, *MNRAS*, 365, 153  
 Cunha, M. S. & Gough, D. 2000, *MNRAS*, 319, 1020  
 Donati, J. F., Catala, C., Landstreet, J. D., & Petit, P. 2006, in *Astronomical Society of the Pacific Conference Series*, Vol. 358, *Solar Polarization 4*, ed. R. Casini & B. W. Lites, 362  
 Donati, J. F., Semel, M., Carter, B. D., Rees, D. E., & Collier Cameron, A. 1997, *MNRAS*, 291, 658  
 Donati, J. F., Semel, M., & Rees, D. E. 1992, *A&A*, 265, 669  
 Dziembowski, W. A. & Goode, P. R. 1996, *ApJ*, 458, 338  
 Erspamer, D. & North, P. 2003, *A&A*, 398, 1121  
 Folsom, C. P., Bouvier, J., Petit, P., et al. 2018, *MNRAS*, 474, 4956  
 Gaia Collaboration, Brown, A. G. A., Vallenari, A., et al. 2018, *A&A*, 616, A1  
 Gaia Collaboration, Prusti, T., de Bruijne, J. H. J., et al. 2016, *A&A*, 595, A1  
 Gaia Collaboration, Vallenari, A., Brown, A. G. A., et al. 2023, *A&A*, 674, A1  
 Ghazaryan, S., Alecian, G., & Hakobyan, A. A. 2018, *MNRAS*, 480, 2953  
 Gray, R. O., Corbally, C. J., De Cat, P., et al. 2016, *AJ*, 151, 13  
 Grevesse, N. & Sauval, A. J. 1998, *Space Sci. Rev.*, 85, 161

- Holdsworth, D. L. & Brunsten, E. 2020, *PASP*, 132, 105001  
 Holdsworth, D. L., Kurtz, D. W., Smalley, B., et al. 2016, *MNRAS*, 462, 876  
 Holdsworth, D. L., Saio, H., Bowman, D. M., et al. 2018, *MNRAS*, 476, 601  
 Huber, D., Silva Aguirre, V., Matthews, J. M., et al. 2014, *ApJS*, 211, 2  
 Hümmerich, S., Mikulášek, Z., Paunzen, E., et al. 2018, *A&A*, 619, A98  
 Koch, D. G., Borucki, W. J., Basri, G., et al. 2010, *ApJ*, 713, L79  
 Kochukhov, O. 2003, *A&A*, 404, 669  
 Luo, A. L., Zhao, Y. H., Zhao, G., & et al. 2022, *VizieR Online Data Catalog*, V/156  
 Mathys, G. 1989, *Fund. Cosmic Phys.*, 13, 143  
 Matsuno, T., Starkeburg, E., Balbinot, E., & Helmi, A. 2022, *arXiv e-prints*, arXiv:2212.11639  
 Pinsonneault, M. H., An, D., Molenda-Żakowicz, J., et al. 2012, *ApJS*, 199, 30  
 Preston, G. W. 1974, *ARA&A*, 12, 257  
 Rees, D. E. & Semel, M. D. 1979, *A&A*, 74, 1  
 Ricker, G. R., Winn, J. N., Vanderspek, R., et al. 2015, *Journal of Astronomical Telescopes, Instruments, and Systems*, 1, 014003  
 Ryabchikova, T., Piskunov, N., Kurucz, R. L., et al. 2015, *Physica Scripta*, 90, 054005  
 Saio, H. 2005, *MNRAS*, 360, 1022  
 Saio, H. & Gautschi, A. 2004, *MNRAS*, 350, 485  
 Shi, F., Kurtz, D., Saio, H., Fu, J., & Zhang, H. 2020, *ApJ*, 901, 15  
 Sneden, C., Bean, J., Ivans, I., Lucatello, S., & Sobeck, J. 2012, *Astrophysics Source Code Library*, 02009  
 Stibbs, D. W. N. 1950, *MNRAS*, 110, 395  
 Xiang, M., Rix, H.-W., Ting, Y.-S., et al. 2022, *A&A*, 662, A66  
 Zhao, G., Zhao, Y.-H., Chu, Y.-Q., Jing, Y.-P., & Deng, L.-C. 2012, *Research in Astronomy and Astrophysics*, 12, 723

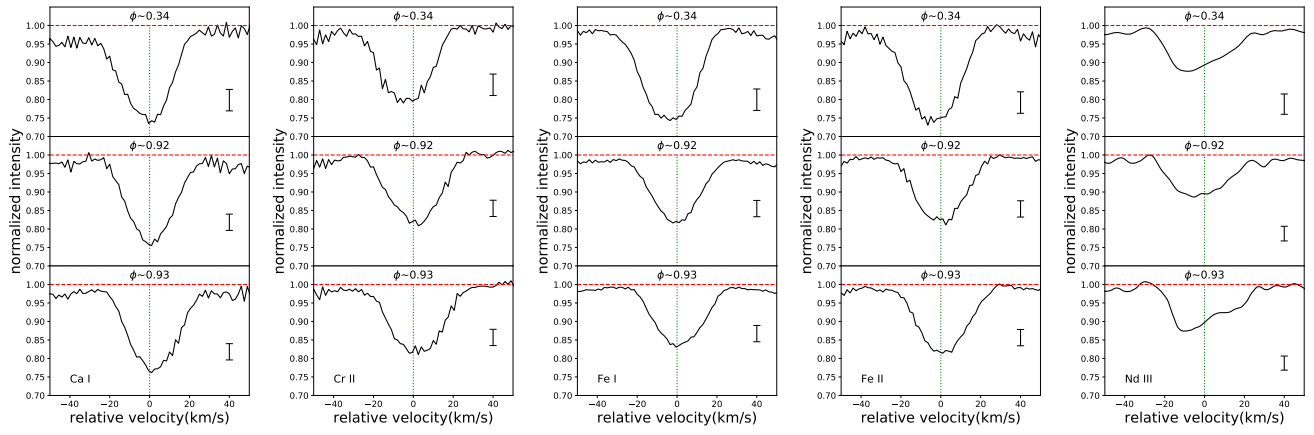


Fig. 7: Same as Fig. 6 but for different elements. The rotation phases are marked at the top of each panel. For Nd III, the intensity profiles of 6145.07 Å are directly compared, instead of calculating LSD profiles.